12th IFAC International Symposium on
Advanced Control of Chemical Processes
July 14-17, 2024. Toronto, Canada

Robust tube-based predictive control of continuous protein production by purple non-sulfur bacteria

Matheus C. R. Nunes * **Laurent Dewasme** * **Manon Gilson** **
Guillaume Bayon-Vicente ** **Baptiste Leroy** ** **Alain Vande Wouwer** *

* *Systems, Estimation, Control and Optimization (SECO), University of Mons, Belgium (e-mail: matheus.camargoromanonunes@umons.ac.be, laurent.dewasme@umons.ac.be, alain.vandewouwer@umons.ac.be).*
** *Laboratory of Proteomics and Microbiology, University of Mons, Belgium (e-mail: manon.gilson@umons.ac.be, guillaume.bayon-vicente@umons.ac.be, baptiste.leroy@umons.ac.be).*

Abstract: A tube-based nonlinear model predictive controller (NMPC) is developed to regulate a continuous bioprocess of purple non-sulfur bacteria (PNSB). The controller employs a macroscopic model that exhibits significant parametric uncertainty due to the restricted availability of experimental data for parameter identification. The proposed model describes microbial protein production during PNSB growth on fructose and glucose. This work aims to assess the robustness of the proposed control strategy and compare the performance with classical NMPC. To this end, both controllers are challenged in a Monte-Carlo study, with identical disturbances in the form of parametric variations spread over 100 different scenarios. The resulting trajectories, as well as biomass and protein productivity levels, confirm the better performance of the robust tube-based controller.

Keywords: model predictive control, process control, parameter estimation, biotechnology, chemostat.

1. INTRODUCTION

Purple non-sulfur bacteria (PNSB) are versatile organisms capable of, under anaerobic conditions, phototrophically consuming various carbon sources, such as carbohydrates (Kars and Alparslan, 2013), amino acids (Teixeira et al., 2010), and volatile fatty acids (VFA) (Cabecas Segura et al., 2022a). Industrial interest in PNSB has been increasing in recent years due to their unique feature of converting industrial or domestic waste streams into higher value components, including microbial protein (MP), also called single-cell protein (SCP), carotenoids, coenzyme Q10, hydrogen, and bioplastics (Capson-Tojo et al., 2020). Among these, MP constitutes a promising alternative to complement human (Alloul et al., 2019; Spanoghe et al., 2021) or animal feed (Delamare-Debouteville et al., 2019). Despite the clear potential, current technological challenges must be addressed to make PNSB commercially feasible. Capson-Tojo et al. (2020) have identified areas of improvement related to process design, process efficiency (light and substrate conversion), and product valorization. Considering this context, the definition of an advanced control structure to regulate the formation of a targeted product by PNSB may as well be a valuable resource for an industrial scale-up.

In this regard, nonlinear model predictive control (NMPC) is an appealing approach, also considering the reported applications to bioprocess control in the literature. Particular strategies can be adopted according to specific control objectives, like maximization of biomass production (Santos et al., 2012) or a specific product (Dewasme et al., 2023), substrate regulation (Craven et al., 2014), or trajectory tracking (Ulonska et al., 2018). NMPC, however, relies on the development of a model, which may be a complex task. Data collection requires a series of batch or fed-batch experiments, which are commonly costly and time-consuming. Also, even if a large amount of data is available, the impact of the remaining parametric uncertainties may still need to be accounted for. For this reason, a considerable research effort is directed to robust NMPC where modeling uncertainties are handled, from conservative approaches such as minimax MPC (Santos et al., 2012; Dewasme et al., 2015) to tube-based (Mayne et al., 2011; Zhong et al., 2023; Dewasme et al., 2024), multi-stage (Hebing et al., 2020; Dewasme et al., 2023), and stochastic MPC (Mesbah, 2016).

The next section presents a mechanistic model describing the evolution of *Rs. rubrum*, focusing on protein production. The motivation for considering the significant parametric uncertainty levels is supported by the possible lack of economic resources to produce more data. Even though some models describing the growth of purple bacteria are already reported (Puyol et al., 2017; Cabecas Segura et al., 2022a,b; Capson-Tojo et al., 2023), none of them have all the attributes required for this study, i.e. PNSB growth exclusively on glucose and fructose combined with protein production. A different model is therefore proposed to fulfill this purpose. Section 3 presents the control problem and the classical and tube-based NMPC designs. The robustness of both controllers with respect to parameter uncertainties is assessed and discussed. Conclusions are drawn in section 4, regarding what is, to the best of the authors' knowledge, the first advanced control work dedicated to PNSB.

2. MATHEMATICAL MODEL OF PNSB GROWTH

2.1 Model description

A dynamic model is proposed to describe *Rs. rubrum* growth on fructose and glucose, both generated by sucrose hydrolysis

and coupled with intracellular protein production. The reaction scheme and substrate kinetics are respectively inspired by Cabecas Segura et al. (2022a) and Fekih-Salem et al. (2019). The resulting macro-reactions read as follows:

$$Y_f\, fru \xrightarrow{\varphi_1} X + Yp_1 P \tag{1}$$

$$Y_g\, glu \xrightarrow{\varphi_2} X + Yp_2 P \tag{2}$$

where X, fru, glu, and P, are, respectively, the concentrations of biomass (g L^{-1}), fructose (g L^{-1}), glucose (g L^{-1}), and protein (g L^{-1}). Y_f, Y_g, Yp_1, and Yp_2 respectively correspond to the fructose, glucose, and protein yield coefficients.

The reaction rates, defined as Monod-type kinetics, are given by:

$$\varphi_1 = \mu_{\max_1} X \frac{fru}{K_1 + fru} \tag{3}$$

$$\varphi_2 = \mu_{\max_2} X \frac{glu}{K_2 + glu} \tag{4}$$

where $\mu_{\max_1}$ and $\mu_{\max_2}$ are the maximum specific growth rates and K_1 and K_2 are the half-saturation constants of fructose and glucose, respectively. Protein production is described as a regular bioprocess product, following the structure of product formation described in Bastin and Dochain (1990).

Applying mass balances for each component and considering a chemostat operating mode leads to the following differential equations:

$$\frac{dX}{dt} = \varphi_1 + \varphi_2 - \frac{F}{V}X \tag{5}$$

$$\frac{dfru}{dt} = -Y_f\varphi_1 + \frac{F}{V}(fru_{in} - fru) \tag{6}$$

$$\frac{dglu}{dt} = -Y_g\varphi_2 + \frac{F}{V}(glu_{in} - glu) \tag{7}$$

$$\frac{dV}{dt} = 0 \tag{8}$$

$$\frac{dP}{dt} = Yp_1\varphi_1 + Yp_2\varphi_2 - \frac{F}{V}P \tag{9}$$

where F is the inlet flow of the reactor and V is the reactor's constant volume. The dilution rate in h^{-1} is defined by $D = F/V$, and the productivity of biomass and protein, in g L^{-1} h^{-1}, are calculated as $Prod_X = DX$, and $Prod_P = DP$.

2.2 Model identification and validation

Parameter identification and sensitivity analysis are performed using a procedure inspired from Fekih-Salem et al. (2019). The parameters are estimated by weighted least-squares, while the sensitivity analysis allows the evaluation of the Fisher Information Matrix (FIM), and in turn, the confidence intervals for each parameter.

The database is composed of 6 batch experiments where only 2 of them provide protein concentration data. A more thorough discussion of the experimental conditions, the measurement analytical devices, and the metabolic features of *Rs. rubrum* will be reported elsewhere.

Fig. 1 shows the model prediction for the first 4 batch experiments without protein concentration measurements (direct validation with the data used for identification), while Fig. 2 shows the direct validation with the 2 remaining experiments where measurements of the protein concentrations are available. The estimated parameters, along with their 95% confidence intervals, are listed in Table 1. In view of the limited amount of available data, it is not a surprise that some of these confidence intervals are quite large. It should also be noted that model reduction (for instance, merging both reaction rates) unfortunately degrades curve fitting. Moreover, no other kinetic structure, for instance including inhibition factors, could improve the root mean square errors (RMSEs) shown in Table 2.

The large confidence intervals related to fructose consumption are explained by the fast nutrient exhaustion highlighted in Fig. 1, resulting in a small number of non-zero data. After complete fructose depletion, biomass growth relies solely on glucose.

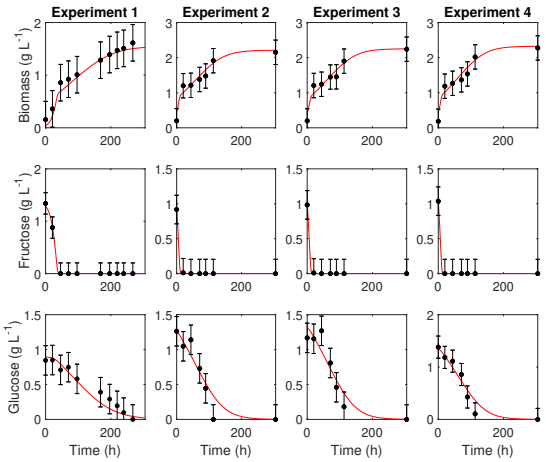

Fig. 1. Model predictions (red continuous line) for the concentrations of biomass, fructose, and glucose in experiments 1-4, and experimental data (black dots). The bars correspond to *a posteriori* calculations of the 95% confidence intervals related to the measurement error.

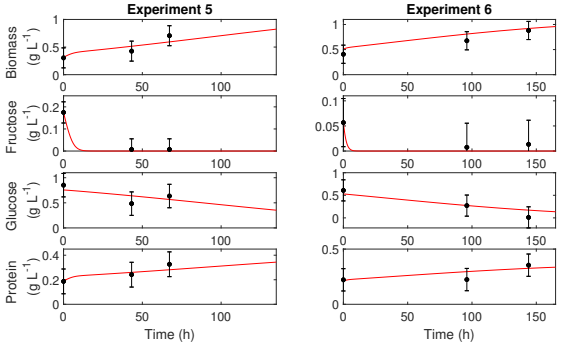

Fig. 2. Model predictions (red continuous line) for the concentrations of biomass, fructose, glucose, and protein in experiments 5-6, and experimental data (black dots). The bars correspond to *a posteriori* calculations of the 95% confidence intervals related to the measurement error.

One can also notice that the uncertainty related to one of the protein yield coefficients (Yp_2) is significantly higher than the other (Yp_1), which might suggest the possibility of a model reduction. Since it is observed that protein formation is correlated to biomass concentration (Fig. 2), the available information is not sufficient to support the decision to remove one of these

yield coefficients. However, despite these parametric uncertainties, the RMSEs given in Table 2 are acceptable. Hence, these parameter uncertainties confirm the requirement for a robust control framework.

Table 1. Estimated parameters, standard deviations, and confidence intervals.

Parameter	Estimated value	Standard deviation (σ)	CI (%)
μ_{max_1} (h^{-1})	0.0838	0.267	636
μ_{max_2} (h^{-1})	0.0198	0.009	95.0
K_1 (g L^{-1})	0.181	4.08	4514
K_2 (g L^{-1})	1.40	1.05	150
Y_f (g g^{-1})	2.37	0.373	31.0
Y_g (g g^{-1})	0.925	0.0807	17.0
Yp_1 (g g^{-1})	0.496	0	0
Yp_2 (g g^{-1})	0.269	1.33	985

Table 2. RMSE results for biomass, fructose, glucose, and protein.

Component	RMSE
X	0.125
fru	0.0133
glu	0.123
P	0.0270

3. TUBE-BASED MODEL PREDICTIVE CONTROL

3.1 Formulation of the control problem

As biological systems are inherently uncertain, robust control represents an effective approach to minimize the effect of parameter variability. Tube-based nonlinear model predictive control, as proposed by Mayne et al. (2011), offers a solution by reducing the dispersion of the trajectories of a system subject to a priori unknown disturbances. This cascade control strategy proceeds in two steps, first determining a (often off-line) nominal optimal trajectory (also called central path), based on the resolution of an optimization problem using the non-disturbed process model. A second optimization is then achieved by an ancillary controller, preventing the state and input variables from making important deviations from the central path, and therefore maintaining all trajectories in their respective robust sets, also called tubes. Computing the tubes is challenging in the specific case of nonlinear systems. An approximation can however be achieved through a Monte-Carlo analysis (Mayne et al., 2011).

In the following, a tube-based NMPC is designed, where glucose is selected as the controlled variable. The process input is a single feed containing both glucose and fructose, and the process is operated in continuous mode at constant volume (chemostat).

The nominal NMPC problem, at instant $i \in [0, t_f]$, is formulated as:

$$J_{nom} = \arg\min_{v} \sum_{t=i}^{i+p} (glu_z(t) - glu_{\text{ref}}(t))^2 \tag{10}$$

$$s.t. \quad \dot{z} = f(z(t), v(t), \theta; z_{0,i}), \quad t \in [i, i+p] \tag{11}$$

$$v_{\min} \leq v(t) \leq v_{\max} \tag{12}$$

where $z = [X_z \; fru_z \; glu_z \; V_z \; P_z]$ is the nominal state vector (the index z also stands for nominal state variables), v is the nominal input variable, θ is the vector of nominal parameters, and $z_{0,i}$ is the vector of nominal initial states at instant $t = i$. The nominal optimal glucose and input flow rate trajectories, obtained by solving (10-12), are respectively denoted glu_z^* and v^*. p is the prediction horizon and glu_{ref} is the glucose setpoint, which is initially fixed to 0.45 g L^{-1} until 720 h. After 720 h, a glucose reference step change to 0.30 g L^{-1} is applied and maintained until the end of the experiment (at the final time $t_f = 1200\ h$). The input constraints related to the feed rate are $v_{\min} = 0$ and $v_{\max} = 0.0171$ L h^{-1} (representing the limits of the pump), and the reactor volume V is constant and equal to 2 L. The initial concentrations of biomass, fructose, glucose, and protein are, respectively, 0.236, 0.373, 0.591, and 0.156 g L^{-1}. The concentrations of fructose and glucose in the single feed are 1.07 and 1.16 g L^{-1}. The prediction horizon and control horizon are both set to p=120 h, and the sampling time T_s is 24 h. Except for the nominal case, a white noise level with 3% standard deviation is added to the state variable measurements in all simulations.

The selection of glucose as the target variable, as well as the sampling time T_s, are motivated by the extensive literature regarding bioprocess control with glucose regulation. Considering that bioprocess are usually characterized by slow dynamics, Craven et al. (2014) discuss the implementation of an NMPC scheme for regulating glucose concentrations with long measurement intervals (12 h) under the presence of noise and process variability, to replicate an industrial operation and assess the feasibility of an at- or off-line application. In the referenced study, the successful performance of the controller is verified by comparing the off-line measurements used by the NMPC to those acquired online at 6 min intervals. If the process is slow enough, measurement techniques such as high-performance liquid chromatography (HPLC) can be employed, with a longer sampling time (Ulonska et al., 2018). The usual online availability of biomass and glucose measurements also allows considering the use of a soft sensor (observer), as in Dewasme et al. (2015).

The control problem formulated in (11) to (12) is solved with the nonlinear Model Predictive Control toolbox from Matlab®. This tool allows the definition of an NMPC object containing the parameters of the control problem. The optimization problem is solved by applying the function *nlmpcmove* at each time sample. Simulation results for the nominal (non-disturbed) MPC lead to a successful regulation as highlighted in Figs. 3 and 4.

3.2 Classical NMPC vs tube-NMPC application

This section is devoted to the robustness analysis of the applications of both classical and tube-based NMPC, subject to identical disturbances in the form of parametric uncertainties assumed to be bounded within the confidence interval ranges. This is achieved by a Monte-Carlo analysis, where the values of nominal parameters θ are randomly varied within their 95% confidence intervals. The sets of parameters θ_j^* for each run j is contained in the range:

$$\theta - 2\sigma \leq \theta_j^* \leq \theta + 2\sigma, \quad j \in \mathbb{N} \mid 1 \leq j \leq 100 \tag{13}$$

where σ is the vector of parametric standard deviations, shown in Table 1. To provide a fair comparison of both controller performances, a tightened constraint NMPC formulation is proposed, where the state constraint

$$glu_{\min} \leq glu_z(t) \leq glu_{\max} \tag{14}$$

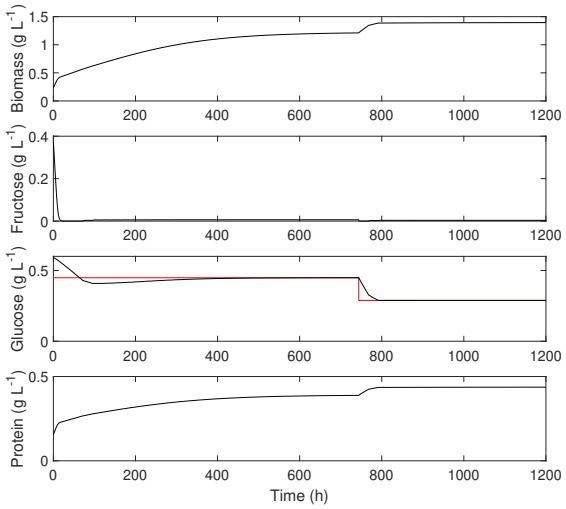

Fig. 3. Nominal NMPC simulation. The black continuous lines indicate the state evolution and the continuous red lines represent the tracked references.

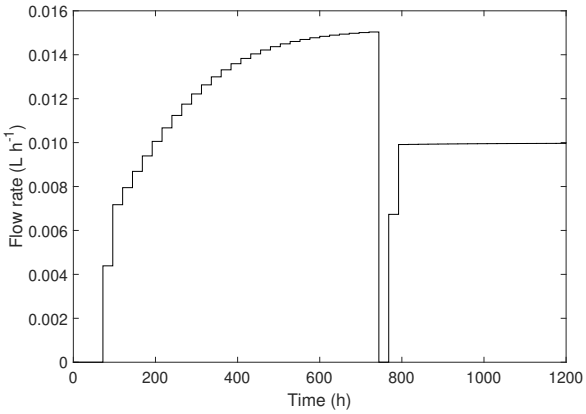

Fig. 4. Feed rate trajectory of the nominal case.

comes in addition to the nominal problem (10-12). The lower and upper bounds of the glucose concentration constraints $glu_{\min}$ and $glu_{\max}$, from (15), are set to $glu_{\min} = glu_{\text{ref}} - 0.07$ g L^{-1} and $glu_{\max} = glu_{\text{ref}} + 0.07$ g L^{-1}. When solving the classical NMPC problem, the process measurements vector at instant t = i, $x_{0,i}$, replaces $z_{0,i}$ in (11).

Figs. 5 and 6 show the state and input evolutions obtained during the Monte-Carlo analysis when using the classical NMPC. The parametric variations lead to a significant spread of the trajectories, poor glucose regulation performance, and constraint violations.

To overcome these issues, a tube-based formulation is adopted, and the following additional ancillary control problem is solved for the j^{th} Monte-Carlo scenario at instant $i \in [0, t_f]$:

$$\min_{u} \quad a \sum_{t=i}^{i+p} (glu_x(t) - glu_z^*(t))^2 + b \sum_{t=i}^{i+p} (u(t) - v_z^*(t))^2 \qquad (15)$$

$$s.t. \quad \dot{x} = f(x(t), u(t), \theta_j^*; x_{0,i}), \quad t \in [i, i+p] \qquad (16)$$

where glu_x is the glucose trajectory of the perturbed system (16), where x and u are, respectively, the state vector and the

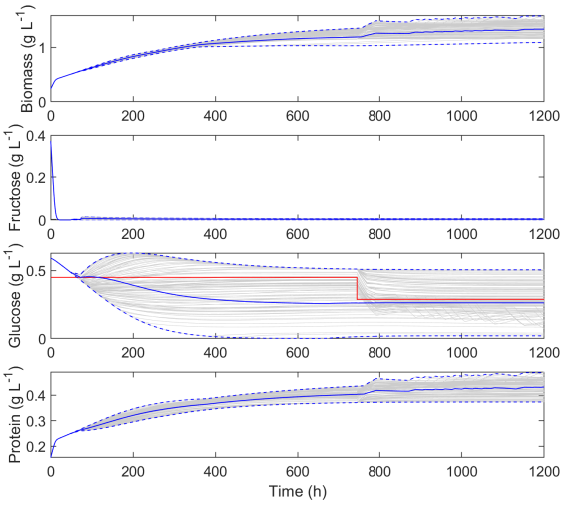

Fig. 5. State evolutions of the classical NMPC simulation for 100 runs, shown in continuous gray lines, with tracking references in continuous red lines. The blue continuous lines are the state mean trajectories, and the blue dashed lines represent the upper and lower corridor bounds.

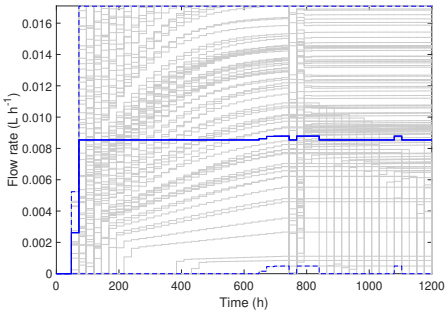

Fig. 6. Gray lines show the feed rate results for 100 runs of the classical NMPC implementation. The blue continuous line is the input mean trajectory, and the blue dashed lines represent the upper and lower corridor bounds.

input of the disturbed system, and $x_{0,i}$ is the process measurement vector at time $t = i$. The solution of the optimal control problem (15-16) leads to the determination of the ancillary optimal glucose concentration glu_x^* and input u^*.

Constraint sets $\mathbb{V}$ and $\mathbb{Z}$ are respectively defined for the nominal input and states. They are subsets of the corresponding perturbed system sets $\mathbb{U}$ and $\mathbb{X}$. Each set is composed of input/state intervals all reported in Tab. 3.

Table 3. States and input intervals on the tube-NMPC application.

Variable	Description	Perturbed system	Nominal system
X	state	[0, 2]	[0.001, 2]
fru	state	[0, 1]	[0.0001, 1]
glu	state	[0, 1]	[0.001, 1]
P	state	[0, 1]	[0.001, 1]
F	input	[0, 0.0171]	[0.000171, 0.0171]

Fig. 7 shows a schematic representation of the tube-NMPC approach, while Figs. 8 and 9 present the results from the application of the proposed strategy to the 100 Monte-Carlo

scenarios, with the same seed of random parametric deviations generated during the classical NMPC applications. Notably, the tube-NMPC highlights better tracking performance, preventing large deviations from the reference. As expected, the ancillary controller forces the trajectories to remain in a tight tube surrounding the reference trajectory. The state and input maximum deviation values confirm this last statement. The standard NMPC trajectories present maximum deviations of 0.25, 0.0077, 0.27, 0.059 g L^{-1}, and 0.0085 L h^{-1}, respectively for X, fru, glu, P, and F. The corresponding tube-NMPC maximum deviations are 0.014, 0.0013, 0.017, 0.0039 g L^{-1}, and 0.0014 L h^{-1}.

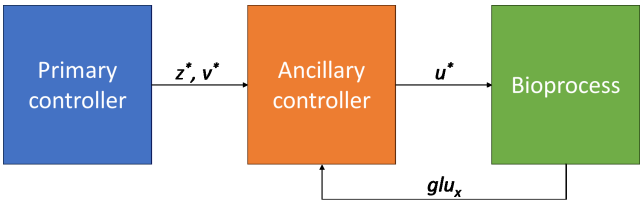

Fig. 7. Tube-NMPC scheme.

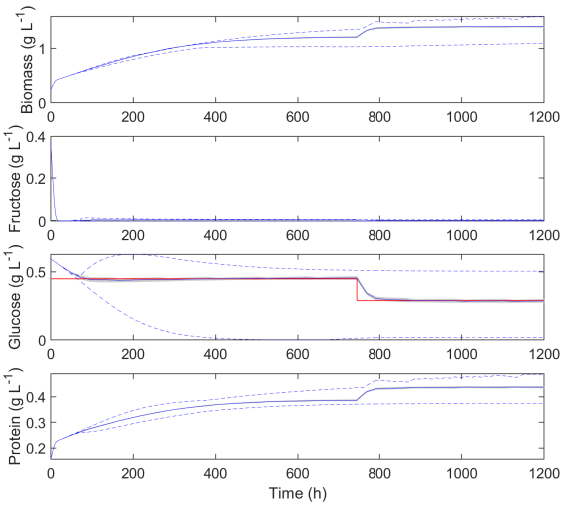

Fig. 8. State evolutions of the tube-NMPC simulation for 100 runs, shown in continuous gray lines, with tracking references in continuous red lines. The blue continuous lines are the state mean trajectories, and the blue dashed lines represent the upper and lower corridor bounds of the classical NMPC application for comparison.

To confirm the latter observations from a quantitative perspective, Figs. 10 and 11 show the distribution of the average biomass ($Prod_X$) and protein ($Prod_P$) productivities over the 100 simulated scenarios.

Overall, biomass productivity values from Fig. 10 indicate a wider dispersion in the classical NMPC cases than in the tube-NMPC cases. A similar outcome can be observed in Fig. 11, in which the predictions for protein productivity are not severely affected by the parametric uncertainty when the tube-based controller is applied, in opposition to the classical one. Tube-NMPC maintains $Prod_X$ within a range from 5.3 $\times$ 10^{-3} to 5.90 $\times$ 10^{-3} g L h^{-1} and $Prod_P$ is estimated to be between 1.80 $\times$ 10^{-3} and 1.90 $\times$ 10^{-3} g L h^{-1}. In comparison, the classical NMPC results for $Prod_X$ are between 1.13 $\times$ 10^{-4}

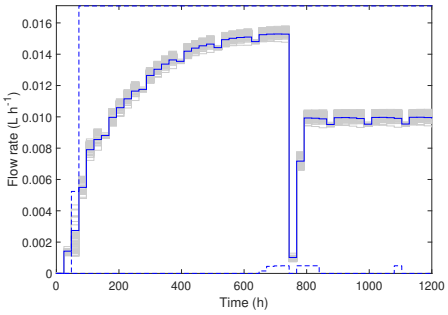

Fig. 9. Gray lines show the feed rate results for 100 runs of the tube-NMPC implementation. The blue continuous line is the input mean trajectory, and the blue dashed lines represent the upper and lower corridor bounds of the classical NMPC application for comparison.

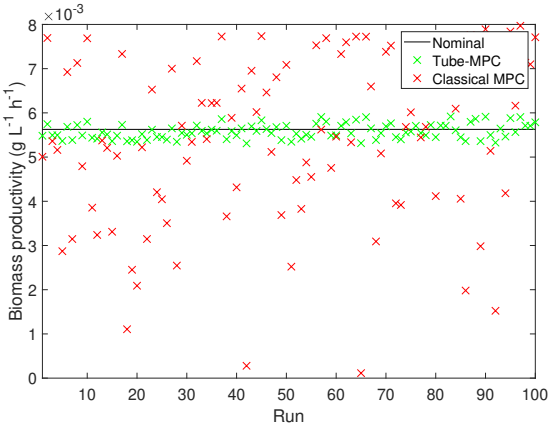

Fig. 10. Average biomass productivity in 100 simulated scenarios. Tube-NMPC results are shown in green markers, classical NMPC values are presented in red markers, and the black continuous line represents the expected results of the nominal case.

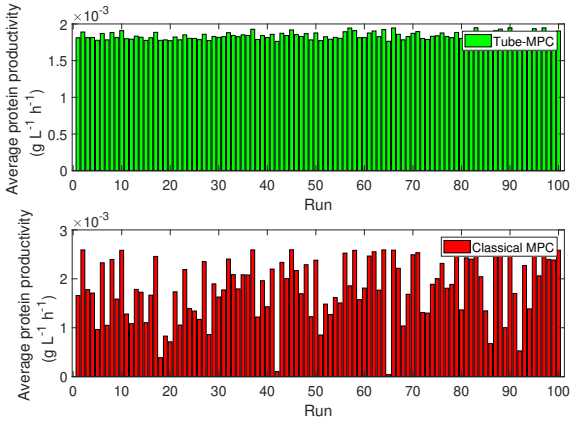

Fig. 11. Average protein productivity in 100 simulated scenarios. Tube-NMPC results are represented by green bars, and classical NMPC is represented by red bars.

and 8.00 $\times$ 10^{-3} g L h^{-1}, while $Prod_P$ goes from 4.23 $\times$ 10^{-5} to 2.70 $\times$ 10^{-3} g L h^{-1}. Therefore, one can infer that a robust tube-NMPC is a suitable alternative for industrial processes focused on MP production by PNSB, given that product stan-

dardization and repeatability should be regarded as essential decision factors for process design and control.

4. CONCLUSION

In this work, a predictive control framework for the substrate regulation of a continuous purple non-sulfur bacteria (PNSB) culture is proposed. A mechanistic model of PNSB growth on glucose and fructose is first identified and validated while exhibiting large parametric uncertainties related to the limited amount of available data. A Monte-Carlo study mapping the parametric variability through 100 scenarios reveals that a classical NMPC formulation fails to maintain the substrate regulation conditions while a tube-based NMPC strategy shows better tracking and robustness performance. Moreover, biomass and protein productivity present minor deviations among all the performed Monte-Carlo runs. Future work should focus on the collection of data to consolidate the model, as well as on identification and robust control applications directed to other strains of PNSB presenting more complex scenarios, such as considering additional controlled and input variables.

ACKNOWLEDGEMENTS

The research leading to these results has been funded by the Public Service of Wallonia (Economy, Employment and Research), under the FoodWal agreement n°2210182 from the Win4Excellence project of the Wallonia Recovery Plan.

REFERENCES

Alloul, A., Wuyts, S., Lebeer, S., and Vlaeminck, S.E. (2019). Volatile fatty acids impacting phototrophic growth kinetics of purple bacteria: paving the way for protein production on fermented wastewater. *Water Research*, 152, 138–147.

Bastin, G. and Dochain, D. (1990). *On-Line Estimation and Adaptive Control of Bioreactors*. Volume 1 of Process Measurement and Control, Elsevier: Amsterdam.

Cabecas Segura, P., De Meur, Q., Alloul, A., Tanghe, A., Onderwater, R., Vlaeminck, S.E., Vande Wouwer, A., Wattiez, R., Dewasme, L., and Leroy, B. (2022a). Preferential photoassimilation of volatile fatty acids by purple non-sulfur bacteria: Experimental kinetics and dynamic modelling. *Biochemical Engineering Journal*, 186, 108547.

Cabecas Segura, P., Wattiez, R., Vande Wouwer, A., Leroy, B., and Dewasme, L. (2022b). Dynamic modeling of *Rhodospirillum rubrum* PHA production triggered by redox stress during VFA photoheterotrophic assimilations. *Journal of Biotechnology*, 360, 45–54.

Capson-Tojo, G., Batstone, D.J., Grassino, M., Vlaeminck, S.E., Puyol, D., Verstraete, W., Kleerebezem, R., Oehmen, A., Ghimire, A., Pikaar, I., et al. (2020). Purple phototrophic bacteria for resource recovery: Challenges and opportunities. *Biotechnology Advances*, 43, 107567.

Capson-Tojo, G., Batstone, D.J., and Hülsen, T. (2023). Expanding mechanistic models to represent purple phototrophic bacteria enriched cultures growing outdoors. *Water Research*, 229, 119401.

Craven, S., Whelan, J., and Glennon, B. (2014). Glucose concentration control of a fed-batch mammalian cell bioprocess using a nonlinear model predictive controller. *Journal of Process Control*, 24(4), 344–357.

Delamare-Deboutteville, J., Batstone, D.J., Kawasaki, M., Stegman, S., Salini, M., Tabrett, S., Smullen, R., Barnes, A.C., and Hülsen, T. (2019). Mixed culture purple phototrophic bacteria is an effective fishmeal replacement in aquaculture. *Water Research X*, 4, 100031.

Dewasme, L., Mäkinen, M., and Chotteau, V. (2023). Practical data-driven modeling and robust predictive control of mammalian cell fed-batch process. *Computers & Chemical Engineering*, 171, 108164.

Dewasme, L., Fernandes, S., Amribt, Z., Santos, L., Bogaerts, P., and Vande Wouwer, A. (2015). State estimation and predictive control of fed-batch cultures of hybridoma cells. *Journal of Process Control*, 30, 50–57.

Dewasme, L., Mäkinen, M., and Chotteau, V. (2024). Multivariable robust tube-based nonlinear model predictive control of mammalian cell cultures. *Computers & Chemical Engineering*, 183, 108592.

Fekih-Salem, R., Dewasme, L., Castro, C.C., Nobre, C., Hantson, A.L., and Vande Wouwer, A. (2019). Sensitivity analysis and reduction of a dynamic model of a bioproduction of fructo-oligosaccharides. *Bioprocess and Biosystems Engineering*, 42, 1793–1808.

Hebing, L., Tran, F., Brandt, H., and Engell, S. (2020). Robust optimizing control of fermentation processes based on a set of structurally different process models. *Industrial & Engineering Chemistry Research*, 59(6), 2566–2580.

Kars, G. and Alparslan, Ü. (2013). Valorization of sugar beet molasses for the production of biohydrogen and 5-aminolevulinic acid by *Rhodobacter sphaeroides* OU 001 in a biorefinery concept. *International Journal of Hydrogen Energy*, 38(34), 14488–14494.

Mayne, D.Q., Kerrigan, E.C., Van Wyk, E., and Falugi, P. (2011). Tube-based robust nonlinear model predictive control. *International Journal of Robust and Nonlinear control*, 21(11), 1341–1353.

Mesbah, A. (2016). Stochastic model predictive control: An overview and perspectives for future research. *IEEE Control Systems Magazine*, 36(6), 30–44. doi: 10.1109/MCS.2016.2602087.

Puyol, D., Barry, E., Hülsen, T., and Batstone, D. (2017). A mechanistic model for anaerobic phototrophs in domestic wastewater applications: Photo-anaerobic model (PAnM). *Water Research*, 116, 241–253.

Santos, L.O., Dewasme, L., Coutinho, D., and Vande Wouwer, A. (2012). Nonlinear model predictive control of fed-batch cultures of micro-organisms exhibiting overflow metabolism: assessment and robustness. *Computers & Chemical Engineering*, 39, 143–151.

Spanoghe, J., Vermeir, P., and Vlaeminck, S.E. (2021). Microbial food from light, carbon dioxide and hydrogen gas: kinetic, stoichiometric and nutritional potential of three purple bacteria. *Bioresource Technology*, 337, 125364.

Teixeira, P.F., Wang, H., and Nordlund, S. (2010). Nitrogenase switch-off and regulation of ammonium assimilation in response to light deprivation in *Rhodospirillum rubrum* are influenced by the nitrogen source used during growth. *Journal of Bacteriology*, 192(5), 1463–1466.

Ulonska, S., Waldschitz, D., Kager, J., and Herwig, C. (2018). Model predictive control in comparison to elemental balance control in an *E. coli* fed-batch. *Chemical Engineering Science*, 191, 459–467.

Zhong, Z., del Rio-Chanona, E.A., and Petsagkourakis, P. (2023). Tube-based distributionally robust model predictive control for nonlinear process systems via linearization. *Computers & Chemical Engineering*, 170, 108112.